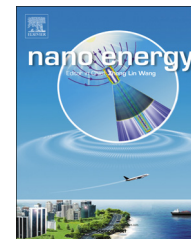


Available online at www.sciencedirect.com

ScienceDirect

journal homepage: www.elsevier.com/locate/nanoenergy

RAPID COMMUNICATION

Orthorhombic niobium oxide nanowires for next generation hybrid supercapacitor device



Xu Wang, Chaoyi Yan, Jian Yan, Afriyanti Sumboja, Pooi See Lee*

School of Materials Science and Engineering, Nanyang Technological University, 639798, Singapore

Received 6 August 2014; accepted 8 November 2014

Available online 15 November 2014

KEYWORDS

Niobium oxide;
Nanowire;
Supercapacitor;
Electrochemistry

Abstract

Energy storage device with high energy density at high power density is of particular importance for various applications, such as hybrid vehicles. Next generation high performance hybrid supercapacitor using organic electrolyte is able to provide high operation voltage as well as enhanced energy density. However, the energy density at high power density is usually low, partly due to the slow electrode kinetics at high current densities. In this contribution, we report a facile preparation method for orthorhombic phase niobium oxide (T-Nb₂O₅) nanowire structure with ultra-thin carbon coating, which shows stable high rate Li⁺ storage ability. A prototype of 3 V hybrid supercapacitor is fabricated using carbon coated T-Nb₂O₅ as anode and commercially available activated carbon as cathode. This hybrid device shows high energy density of 43.4 Wh kg⁻¹ and a high power density of 7.5 kW kg⁻¹ with excellent stability.

© 2014 Elsevier Ltd. All rights reserved.

Introduction

Supercapacitors are a kind of electrochemical energy storage devices, which have attracted much attention due to their high power delivery ability. Electric double layer capacitors (EDLCs) have already been utilized in various applications, such as trucks, buses, elevators as well as heavy duty constructions and railways in powering forklifts and yard cranes [1]. However, the energy density is expected to elevate to double or triple times to 20–30 Wh kg⁻¹ at a certain power

density for various emerging applications so as to penetrate a larger energy storage market. In order to achieve enhanced energy density of supercapacitor, elevated operation potential window is highly demanded, as $E=0.5CV^2$. Though numerous efforts have been spent on developing aqueous electrolyte based hybrid supercapacitor device, the water decomposition will limit the operation window of device less than 2 V. Therefore, organic electrolyte based non aqueous hybrid (asymmetric) supercapacitor is of great interest for its large operation window (>2.5 V).

Lithium ion insertion metal oxide with fast charge storage ability is an ideal choice to develop the hybrid supercapacitor with carbon electrode [2]. They are qualified to provide large amount of charge storage as well as large operation window of

*Corresponding author. Tel.: +65 67906661; fax: +65 679069081.
E-mail address: pslee@ntu.edu.sg (P.S. Lee).

hybrid device. V_2O_5 , [3] $Li_4Ti_5O_{12}$ [4] and $B-TiO_2$ [5] have been explored as electrode materials for non-aqueous hybrid supercapacitors. Generally, the charge storage of these materials contains both instant capacitive (EDLC and pseudocapacitive) charge storage (surface reaction) and diffusion controlled battery-type charge storage (bulk reaction, diffusion controlled). However, due to the low Li^+ diffusion constant in the bulk, the rate capability of these materials is not satisfactory. As a result, the energy densities of those hybrid devices at high power densities are still not satisfactory. For example, though Chen et al. successfully achieved an energy density of 40 Wh kg^{-1} @ 210 W kg^{-1} in a V_2O_5 -CNT//Activated Carbon device, the energy density only remains 7 Wh kg^{-1} @ 6.1 kW kg^{-1} . The low energy density at high power densities would not be favorable for heavy duty or high power delivery operations. In order to achieve better energy density at high power densities, fast electrochemical reaction kinetics of Li^+ diffusion is highly desirable for non-aqueous hybrid supercapacitor.

Recently, orthorhombic phase Nb_2O_5 (T- Nb_2O_5) nanocrystals are found to exhibit fast pseudocapacitive Li^+ storage based on an unique intercalation pseudocapacitance. [6,7] The Li^+ diffusion is proved to have fast kinetics in the bulk material without inducing any phase change [6]. However, the capacities of T- Nb_2O_5 nanocrystals are only around $140\sim 150 \text{ mAh g}^{-1}$ [6,7], even they have high surface areas. Considering the theoretical capacity of 200 mAh g^{-1} for T- Nb_2O_5 , there is plenty of room for improvement in capacity. Besides, the report on Nb_2O_5 based non-aqueous hybrid supercapacitor is still scarce. Wang et al. reports a pseudo hexagonal Nb_2O_5 -CNT composite for hybrid supercapacitor [8]. The energy density drops from 33.4 Wh kg^{-1} to 4 Wh kg^{-1} when the power density increases to 4 kW kg^{-1} . The poor performance is largely caused by the non-optimum phase of Nb_2O_5 . On the other hand, one dimensional nanomaterials are of great interest for fully harnessing the merit of materials in energy storage applications. The short ion diffusion length, facile electron conduction channel as well as ease of electrolyte diffusion would greatly benefit the electrochemical process [9,10]. It is therefore invaluable to synthesize one dimensional T- Nb_2O_5 nanowire to harness its potential for hybrid supercapacitor applications.

Currently, there are limited attempts on the controlled synthesis of Nb_2O_5 nanowire with different phases. Most methods are based on the chemical etching of Nb metal as starting material. For example, the high temperature annealing of Nb sheet under O_2 atmosphere at 1000°C yields M- Nb_2O_5 (monoclinic) nanowire [11], or under Ar at 900°C produces tetragonal Nb_2O_5 nanowire [12]. The long time etching in NH_4F gives H- Nb_2O_5 (pseudo-hexagonal, main product) nanorods with mixed phases [13]. Another method is electrospinning using niobium ethoxide as precursor followed by heat treatment, which produced different phases of Nb_2O_5 (including T- Nb_2O_5) [14]. However, the stability of T- Nb_2O_5 is very poor. The capacity degrades 30% in just 40 cycles at 0.05 A g^{-1} .

Here, we develop an oxalate coordination chemistry route to synthesize ultra-thin H- Nb_2O_5 (pseudo-hexagonal) nanowires using low cost $NbCl_5$ as starting material. The ultra-thin nanowires can be transformed into T- Nb_2O_5 nanowires through heat treatment at 600°C . In addition, a few nanometers thin carbon coating is achieved as the shell of T- Nb_2O_5 nanowire by the carbonization of polydopamine. The carbon coated T- Nb_2O_5

nanowire shows a high rate charge/discharge performance and high rate cycling stability as Li^+ ion storage electrode. The capacity reaches 186.8 mAh g^{-1} @ 0.5 C , while it preserves 140.1 mAh g^{-1} @ 25 C . Meanwhile, the capacity can maintain 82% after 1000 cycles at 5 C . A high performance prototype of 3 V hybrid supercapacitor is fabricated with pseudocapacitive carbon coated T- Nb_2O_5 nanowire and activated carbon. The fast Li^+ storage of T- Nb_2O_5 as well as the fast EDLC of activated carbon ensures high energy density delivery at high power density.

Material and methods

Synthesis of Nb_2O_5 nanowires and T- Nb_2O_5 nanowires

All chemicals were purchased from Sigma and were used as received. Briefly, 0.218 g $NbCl_5$ (0.8 mmol) was added into 20 ml DI water under vigorous stirring to give a white floc. Oxalic acid dehydrate (0.5 g , 4 mmol) was added into the suspension till it became transparent. Finally, 0.28 g hexamethylenetetramine (HMTA, 2 mmol) was added into the above solution. The solution was transferred into a 40 ml Teflon lined autoclave and kept at 180°C for 14 h . After that, the samples were collected by centrifuge and were washed with DI water for several times. The samples were dried in oven at 60°C . T- Nb_2O_5 nanowires were achieved by annealing the sample at 600°C for 3 h . For the growth of Nb_2O_5 nanowires on different substrates, silicon and carbon nanofiber substrates were placed in the autoclaves without any special treatment.

Synthesis of polydopamine derived carbon coated T- Nb_2O_5

15 mg dopamine hydrochloride was dissolved in a 15 ml pH 8.5 buffer of Tris containing 50 mg T- Nb_2O_5 sample. The mixture was allowed to stir at room temperature for 48 h . After that, the product was collected by centrifuge and was washed by DI water for several times. The sample was dried in the oven at 60°C . To carbonize the polydopamine, the dried sample was placed in a tube furnace and heat at 600°C under constant Ar flow for 3 h .

Structure characterizations

The products were characterized using X-ray powder diffractometry (XRD; Shimadzu XRD-6000, Cu K α radiation) at a scan rate of 2° min^{-1} , scanning electron microscopy (FESEM; JEOL, JSM-7600 F) and transmission electron microscopy (TEM; JEOL, JEM-2100 F). N_2 adsorption/desorption was determined by Brunauer-Emmett-Teller (BET) measurements using TriStar II surface area and porosity analyzer.

Electrochemical characterization

Activated carbon was purchased from XinSen Carbon Industry Co., Ltd, with a BET surface area of $2084.15 \text{ m}^2 \text{ g}^{-1}$. The working electrode was prepared by mixing $80 \text{ wt.}\%$ active material, $10 \text{ wt.}\%$ carbon black, and $10 \text{ wt.}\%$ polyvinylidene fluoride (PVDF) in NMP. The mixture was then stirred overnight

and the slurry was loaded on the stainless steel coins (1 cm^2 in area) and dried in vacuum oven at $80\text{ }^\circ\text{C}$ for 6 h. The loading mass of active material was acquired by measuring electrode with a microbalance with the accuracy of 0.01 mg. Typically, the loading mass of active material was around 2.0 mg for T-Nb₂O₅ and C-T-Nb₂O₅. The electrode was assembled in CR2032 Coin cell using an Ar filled glovebox with Li disk as both reference and counter electrode, and 1 M LiPF₆ dissolved in 1:1 v/v mixture of ethylene carbonate/diethyl carbonate (EC/DEC) was employed as the electrolyte. The cyclic voltammetry tests were conducted using Autolab PGSTAT 30 potentiostat from 1~3 V. The electrochemical impedance spectrum was recorded using Autolab PGSTAT 30 potentiostat at open circuit potential of activated cell from 10^5 Hz to 0.1 Hz with AC amplitude of 10 mV. The galvanostatic charge-discharge tests were performed in Neware battery testing system from 1~3 V. Supercapacitor devices were assembled in an Ar filled glovebox using C-T-Nb₂O₅ as anode and activated carbon as cathode in CR2032 coin cells. The cyclic voltammetry and galvanostatic charge-discharge tests of hybrid device were conducted using Autolab PGSTAT 30 potentiostat from 0~3 V.

Results and discussion

Structural characterization

For reference, the as prepared sample is termed as Nb₂O₅ and the sample after $600\text{ }^\circ\text{C}$ annealing in air is termed as T-Nb₂O₅. Carbon coating of T-Nb₂O₅ was achieved by the carbonization of polydopamine on T-Nb₂O₅ in Ar at $600\text{ }^\circ\text{C}$. The sample with carbon coating is labeled as C-T-Nb₂O₅. The XRD patterns in Fig. 1a reveal that the sample Nb₂O₅ is pseudo-hexagonal phase (PDF # 028-0317) as prepared from hydrothermal experiment and could be transformed into highly crystalline orthorhombic phase of T-Nb₂O₅ (PDF # 030-0873) after heat treatment at $600\text{ }^\circ\text{C}$. Furthermore, the phase of C-T-Nb₂O₅ remains orthorhombic phase, which suggests the carbonization of polydopamine would not induce any structural change to the sample. Besides, the low content and low graphitization degree of carbon would not lead to obvious XRD peaks. The SEM images in Fig. 1b clearly show that the as prepared Nb₂O₅ sample clustered into a hierarchical interconnected sphere-like structure. In addition, a closer observation in Fig. 1c shows that the individual sphere is assembled by Nb₂O₅ nanowires, forming a highly porous structure. Furthermore, we have also validated that such synthesis strategy is applicable to various substrates, such as silicon and carbon nanofiber to form well-defined nanowire arrays (Fig. S1). This generic synthesis approach makes Nb₂O₅ nanowires highly versatile and ready for use in other fields. The SEM images of sample T-Nb₂O₅ is shown in Fig. 1d and e. The structures of the nanowires are largely preserved after heat treatment, however, there is a certain extent of structural changes related to the collapse and agglomeration of nanowires during heat treatment. Nonetheless, the T-Nb₂O₅ still gives a satisfactory BET surface area of $98.81\text{ m}^2\text{ g}^{-1}$ with a porosity of $0.16\text{ cm}^3\text{ g}^{-1}$. The SEM image of carbon coated T-Nb₂O₅ sample is shown in Fig. 1f. Comparing with the sample T-Nb₂O₅, there is no distinct change in morphology,

suggesting the carbonization process would not damage the nanowire structure.

Detailed structural examination of sample Nb₂O₅, T-Nb₂O₅ and C-T-Nb₂O₅ were carried out in TEM as shown in Fig. 2. It is evident that sample Nb₂O₅ is assembled by ultrathin nanowires with small diameters less than 20 nm depicted in Fig. 2a. High resolution TEM image of sample T-Nb₂O₅ is shown in Fig. 2b. Both nanowires and fragments of nanowires could be observed in sample T-Nb₂O₅. The diameters of T-Nb₂O₅ nanowires and its fragments are below 20 nm. Combining with the SEM results in Fig. 1d, it suggests that the nanowire structure could be largely preserved when transforming into orthorhombic phase. Such nanowire agglomerates with open voids are beneficial to promote the electrolyte wetting and shorten the Li⁺ diffusion length. In Fig. 2c, homogenous carbon coating with only a few nanometers thickness is observed outside the T-Nb₂O₅ nanowires. It demonstrates the successful coating of carbon on T-Nb₂O₅ samples.

Growth mechanism

It is noteworthy to mention that the formation of Nb₂O₅ nanowires could be greatly influenced by the amount of HMTA during synthesis, as illustrated in Fig. S2. Only HMTA concentration of 0.1 M is able to produce nanowire morphology (Fig. S2d). This phenomenon can be explained as the following. During the reaction, the oxalic acid first coordinates with amorphous Nb₂O₅ to give ionic species of $[\text{NbO}(\text{C}_2\text{O}_4)_2(\text{H}_2\text{O})_2]^-$ and $[\text{NbO}(\text{C}_2\text{O}_4)_3]^{3-}$ in acidic solution ($\text{pH} < 3$) [15]. Under further hydrothermal condition, HMTA will undergo hydrolysis to increase the pH of the system. The ionic species of niobium oxalate become unstable and polymerized into solid Nb₂O₅ when pH rises from 3 to 6.5. Nb₂O₅ could be further dissolved in higher pH environment ($\text{pH} > 6.5$) to give various niobium oxide ionic species, such as $\text{H}_x\text{Nb}_2\text{O}_{18}^{(8-x)-}$, $\text{Nb}_{12}\text{O}_{36}^{12-}$ and $\text{Nb}_6\text{O}_{19}^{8-}$ [15]. Thus, when the oxalic acid concentration was fixed at 0.2 M, increasing the HMTA concentration from 0.02 M to 0.1 M would lead to a greater level of dissociation of niobium oxalate, which promotes the growth of Nb₂O₅ solid, as shown in Fig. S2a~d. In contrast, higher HMTA concentration (0.2 M and 0.5 M) would lead to the dissolution of Nb₂O₅ at higher pH, which would damage the nanowire structure, as shown in Fig. 2e~f. Thus, the growth of Nb₂O₅ nanowire structure requires the control of a desirable pH level in the reaction system.

Electrochemical characterization

The electrochemical studies of T-Nb₂O₅ and C-T-Nb₂O₅ were first carried out in coin cells with Li foil as both counter and reference electrode. The CV curves of sample T-Nb₂O₅ and sample C-T-Nb₂O₅ at the first three cycles are shown in Fig. 3a and Fig. 3c respectively. In the first cycle, sample T-Nb₂O₅ shows two cathodic peaks at 1.43 V and 1.62 V respectively. For sample C-T-Nb₂O₅, the first cycle cathodic peaks locate at 1.45 V and 1.81 V. These anodic peaks could be attributed to the decomposition of electrolyte and formation of stable solid electrolyte interphase (SEI) layer [7,16], as well as the Li⁺ insertion.

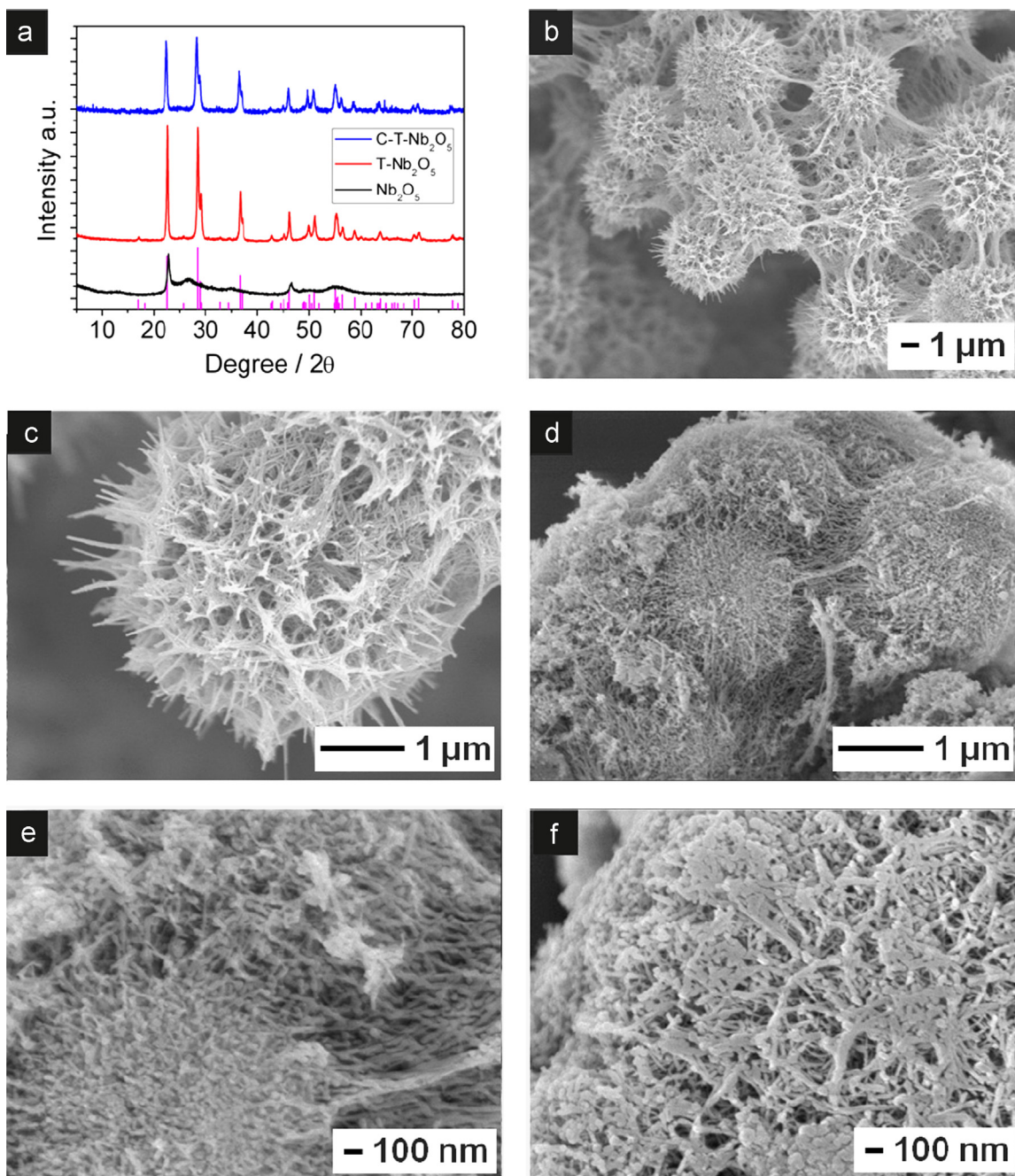
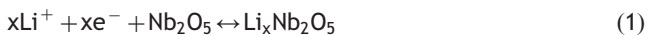


Fig. 1 (a) XRD patterns of sample Nb_2O_5 , $\text{T-Nb}_2\text{O}_5$ and $\text{C-T-Nb}_2\text{O}_5$ (pink lines are the standard diffraction peaks of $\text{T-Nb}_2\text{O}_5$, PDF # 030-0873); (b) and (c) SEM images of sample Nb_2O_5 ; (d) and (e) SEM images of sample $\text{T-Nb}_2\text{O}_5$; (f) SEM image of $\text{C-T-Nb}_2\text{O}_5$.

For both samples, at the 2nd and 3rd cycles, the anodic peaks at 1.53 V and 1.76~1.81 V can be attributed to the reduction of Nb^{5+} to Nb^{4+} and Nb^{3+} (Li^+ intercalation) subsequently, while the cathodic peaks from 1.75 V to 2 V are the result of Li^+ deintercalation from Nb_2O_5 , as shown in Eq. (1) [7, 17]. It is noteworthy to point out that the reduction potential of Nb^{5+} to Nb^{4+} in sample $\text{C-T-Nb}_2\text{O}_5$ is slightly higher comparing to sample $\text{T-Nb}_2\text{O}_5$.



The electrochemical performance of sample $\text{T-Nb}_2\text{O}_5$ and sample $\text{C-T-Nb}_2\text{O}_5$ were further examined by galvanostatic

charge-discharge test. The charge-discharge curves of sample $\text{T-Nb}_2\text{O}_5$ are shown in Fig. 3b. The $\text{T-Nb}_2\text{O}_5$ sample attains a reversible capacity of 209.1 mAh g^{-1} at 0.5 C, which is slightly larger than the theoretical capacity of 200 mAh g^{-1} . The slight increase of reversible capacity could be due to the reversible formation of Li species at low voltage [18]. More significantly, the reversible capacity is able to maintain 160.4 mAh g^{-1} (76.4% retention) even at a current density of 25 C. This clearly demonstrates the high rate capability of $\text{T-Nb}_2\text{O}_5$ sample. On the other hand, the charge-discharge curves of sample $\text{C-T-Nb}_2\text{O}_5$ are shown in Fig. 3d. Due to the inactive carbon coating at the testing

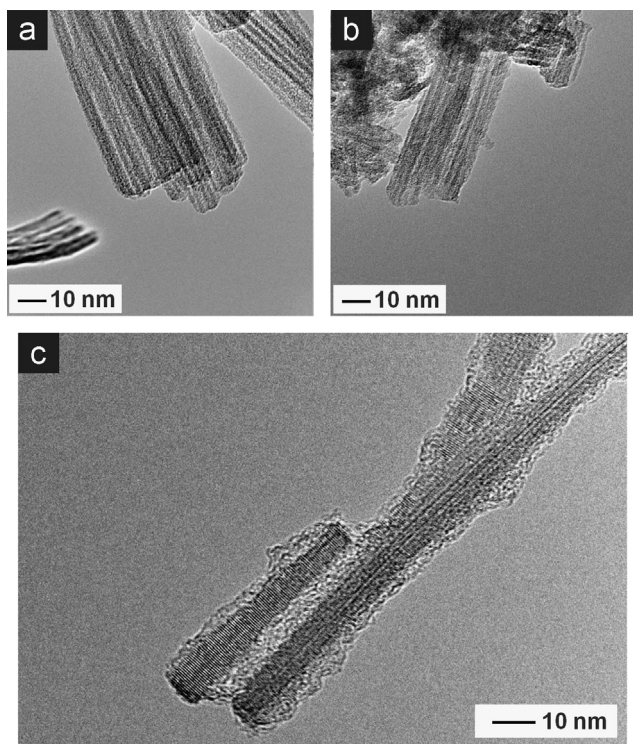


Fig. 2 (a) High magnification TEM image of sample Nb_2O_5 ; (b) high magnification TEM image of sample $\text{T-Nb}_2\text{O}_5$; (c) high magnification TEM image of sample $\text{C-T-Nb}_2\text{O}_5$.

range, this sample shows a lower capacity of 186.8 mAh g^{-1} at 0.5 C , and maintains 140 mAh g^{-1} at 25 C (75% retention). Considering the carbon content of 9.01% determined by TGA in Fig. S3, the capacity of Nb_2O_5 itself remains unchanged ($\sim 205.1 \text{ mAh g}^{-1}$). Meanwhile, similar rate performance could be observed for $\text{T-Nb}_2\text{O}_5$ and $\text{C-T-Nb}_2\text{O}_5$, which indicates that the fast Li^+ intercalation/deintercalation process is not affected by the carbon coating.

The long term cycling stability is critical in device application. Especially in supercapacitor application, up to 1000 cycles are necessary to demonstrate the reliability of materials. However, in previous reports only less than 100 cycles at low current density were demonstrated [13,19]. To demonstrate the stability for fast charge-discharge application, the galvanostatic charge-discharge test of pre-activated cell was carried out at 1 A g^{-1} (5 C) for 1000 cycles. As shown in Fig. 3e, the capacity of sample $\text{T-Nb}_2\text{O}_5$ slightly increased at first 40 cycles then experienced a dramatic fading within the next 160 cycles (32% loss). At last, 53.5% retention could be achieved after 1000 cycles. Such capacity fading characteristic has also been reported by Wang et. al. for pseudo hexagonal Nb_2O_5 (tested up to 500 cycles) [8], a clear reason was not identified yet. On the other hand, the capacity of sample $\text{C-T-Nb}_2\text{O}_5$ shows much better stability, which maintains 82% after 1000 cycles.

To further elucidate the change in the electrochemical behaviors in sample $\text{T-Nb}_2\text{O}_5$ and sample $\text{C-T-Nb}_2\text{O}_5$ after cycling test, electrochemical impedance spectrum (EIS) was carried out as the Nyquist plots shown in Fig. 3f. The carbon coated $\text{T-Nb}_2\text{O}_5$ sample shows reduced equivalent series resistance (ESR), as the first intercept with real axis is

smaller than that of sample $\text{T-Nb}_2\text{O}_5$ [20,21]. More importantly, the radius of the semi-circle in sample $\text{C-T-Nb}_2\text{O}_5$ is much smaller than that of $\text{T-Nb}_2\text{O}_5$, showing a much lower charge transfer resistance of faradic reaction [20,21]. Thus, the carbon coating on $\text{T-Nb}_2\text{O}_5$ helps to lower the ESR of the testing cell as well as reduce the charge transfer resistance during the prolonged tests. In previous studies, Kim et al. and Augustyn et al. have pointed out that the Li^+ ion exhibits fast diffusion in the bulk of $\text{T-Nb}_2\text{O}_5$, whereas the specific origin is still unclear [6,7]. It is therefore unlikely the bulk Li^+ diffusion process within the two samples would differ much. Thus, it is likely that the carbon coating helps to reduce the charge transfer resistance of some reactions at electrode-electrolyte interface. Nevertheless, it will need further investigation to fully understand such phenomenon.

Non-aqueous hybrid supercapacitor

To explore the application of sample $\text{C-T-Nb}_2\text{O}_5$ in the non-aqueous hybrid supercapacitor device, a prototype coin cell device was fabricated based on sample $\text{C-T-Nb}_2\text{O}_5$ and commercially available activated carbon (AC). First, the electrochemical performance of AC was investigated. As shown in Fig. S4a, the activated carbon shows a well defined rectangular shape from 2.6 V to 4.2 V vs. Li/Li^+ from 5 to 20 mV s^{-1} , which indicates an ideal behavior of electrochemical double layer capacitance. At high scan rate, the distortion of CV curve may be due to the ohmic resistance and low ionic conductivity of electrolyte. The specific capacitance (C_{sp}) of activated carbon was determined by galvanostatic charge-discharge test, as shown in Fig. S4b. The activated carbon has a C_{sp} of 125.9 F g^{-1} at 0.2 A g^{-1} . For the assembly of hybrid supercapacitor, the optimum mass ratio of $\text{C-T-Nb}_2\text{O}_5$ and activated carbon was calculated using the charge stored (C g^{-1}) at 0.2 A g^{-1} , based on balancing the charge storages in cathode and anode [20,22]. The operation potential of hybrid supercapacitor was investigated at different voltage windows at a constant charge-discharge current density of 0.5 A g^{-1} , as shown in Fig. S5a. All the charge-discharge curves show triangular shapes, suggesting the capacitive behavior of the device. In Fig. S5b, the C_{sp} reaches a maximum of 29.75 F g^{-1} at an operation potential of 3 V .

The galvanostatic charge-discharge test of hybrid supercapacitor device was carried out from 0 to 3 V at various current densities. As shown in Fig. 4a, the charge-discharge curves all give well-symmetric triangle shapes, which suggest a capacitive response of hybrid supercapacitor device [20]. The specific capacitance of the device is calculated based on Eq. (2):

$$C_{sp} = I \Delta t / M \Delta V \quad (2)$$

where I is the discharge current, Δt is the discharge time after IR drop, M is the total mass of both positive and negative electrodes, and ΔV is the potential window of device. As shown in Fig. 4b, the C_{sp} of the device could reach 34.8 F g^{-1} at a current density of 0.25 A g^{-1} , while it maintains 8.7 F g^{-1} at 5 A g^{-1} . To better demonstrate the energy and power characters of $\text{C-T-Nb}_2\text{O}_5//\text{AC}$ hybrid device, Ragone plot is plotted in Fig. 4c according to Eqs.

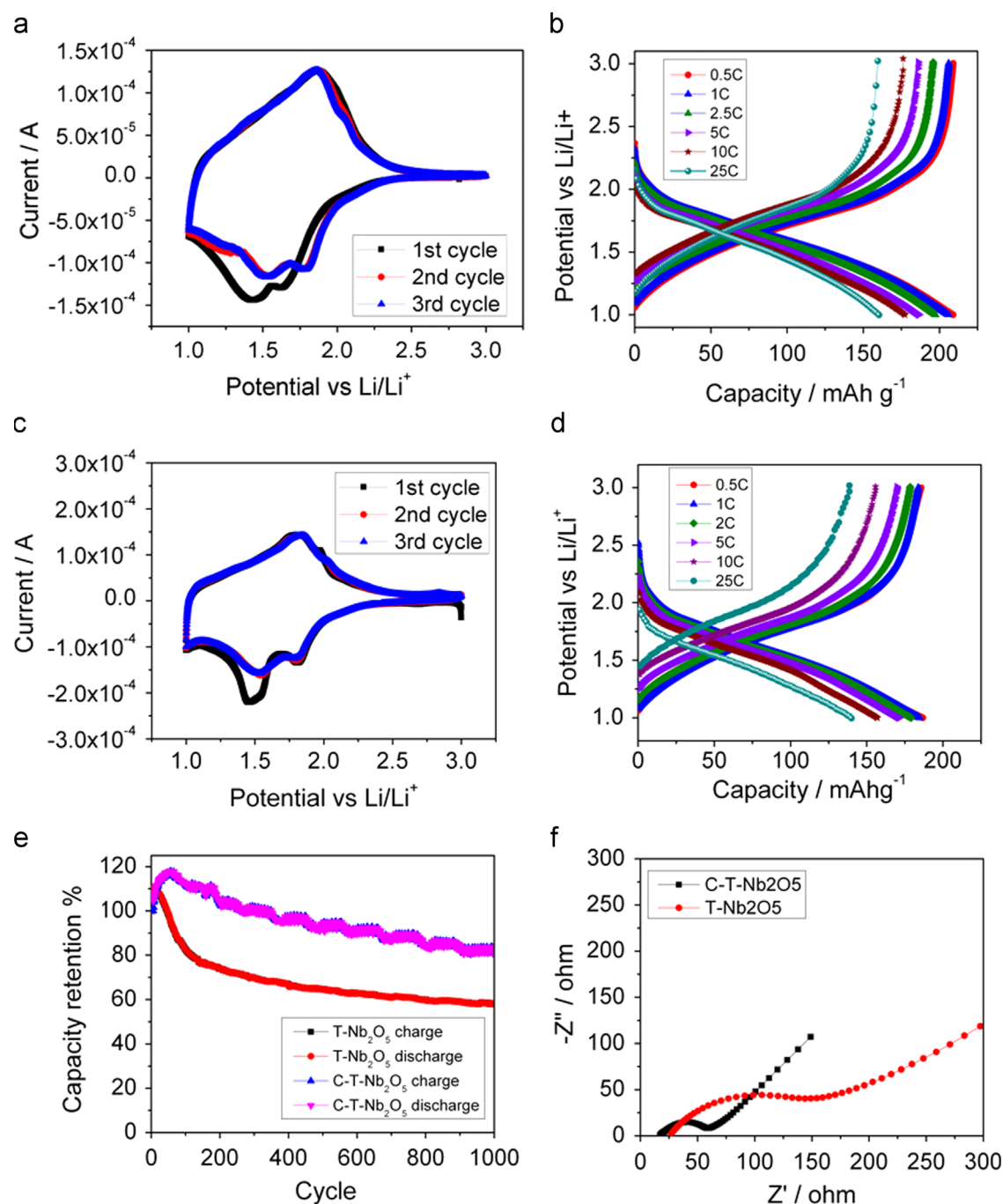


Fig. 3 (a) Cyclic voltammetry curves of sample T-Nb₂O₅ of first 3 cycles at a scan rate of 0.1 mV s⁻¹; (b) charge-discharge curves of sample T-Nb₂O₅ at difference current densities; (c) Cyclic voltammetry curves of sample C-T-Nb₂O₅ of first 3 cycles at a scan rate of 0.1 mV s⁻¹; (d) charge-discharge curves of sample C-T-Nb₂O₅ at difference current densities; (e) relationships between cycle number and capacity retention of sample T-Nb₂O₅ and sample C-T-Nb₂O₅ at a charge-discharge current density of 5 C, data recorded after rate capability tests; (f) Nyquist plots of sample T-Nb₂O₅ and C-T-Nb₂O₅ after cycling tests.

(3) and (4):

$$E = 1/2C_{sp}V^2 \quad (3)$$

$$P = E/t \quad (4)$$

where C_{sp} is the specific capacitance calculated from the charge-discharge test, V is the working potential, and t is

the discharge time. As shown in Fig. 4c, the hybrid device of C-T-Nb₂O₅//AC reaches a high energy density of 43.4 Wh kg⁻¹ at a power density of 374.98 W kg⁻¹ (charge/discharge time ~405.2 s), meanwhile it also maintains a high energy density of 10.8 Wh kg⁻¹ at a power density of 7500 W kg⁻¹ (charge/discharge time ~5.1 s). These values indicate the high power performance of this hybrid device.

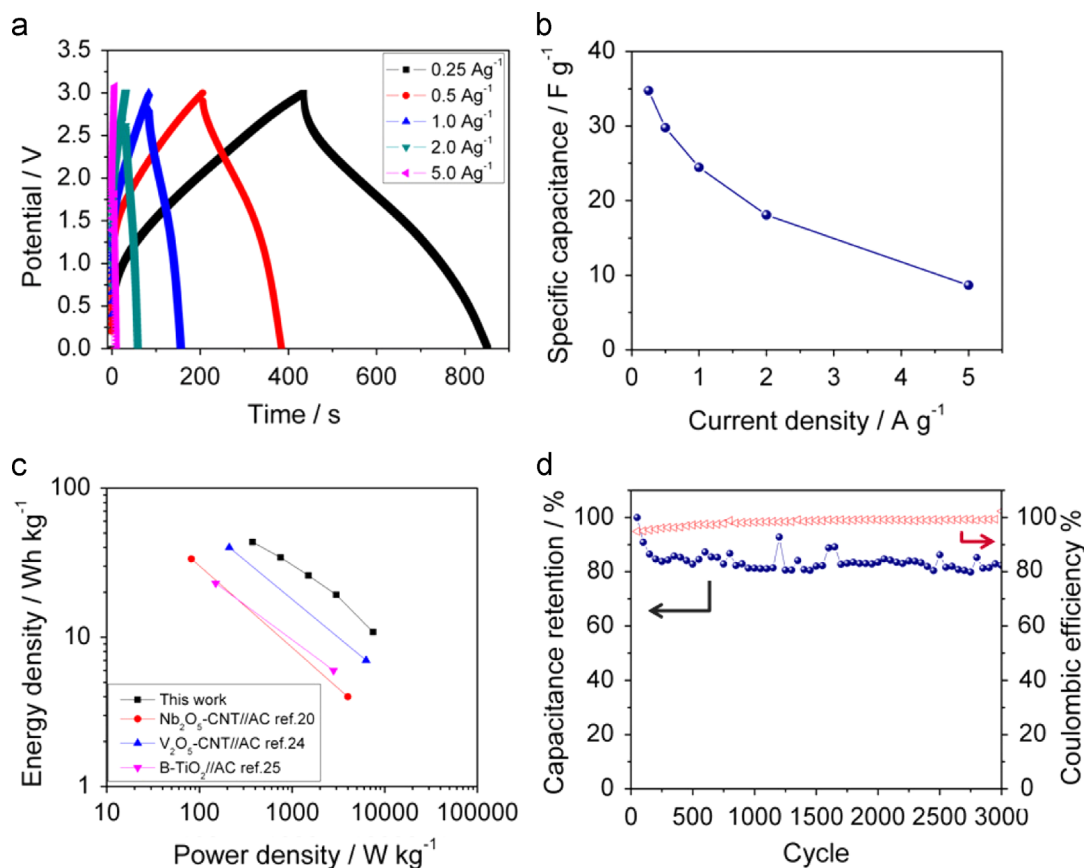


Fig. 4 (a) Galvanostatic charge-discharge curves of C-T-Nb₂O₅//AC hybrid device at different current densities; (b) relationship between current density and specific capacitance of C-T-Nb₂O₅//AC hybrid device; (c) Ragone plot of C-T-Nb₂O₅//AC hybrid device and comparison with recent literature data; (d) relationship between cycle number and capacitance retention and coulombic efficiency at 20 mV s⁻¹.

Furthermore, as shown in Fig. 4c, the hybrid device in this work shows improved energy density at the same power density comparing with previous reports on non-aqueous hybrid supercapacitors, such as Nb₂O₅ nanocrystal-CNT//AC (33.5 Wh kg⁻¹ @82 W kg⁻¹, 4 Wh kg⁻¹ @4000 W kg⁻¹) [8], CNT-V₂O₅//AC (40 Wh kg⁻¹ @210 W kg⁻¹, 7 Wh kg⁻¹ @6300 W kg⁻¹) [3], B-TiO₂//AC (23 Wh kg⁻¹ @150 W kg⁻¹, 6 Wh kg⁻¹ @2800 W kg⁻¹) [5]. Therefore, it demonstrates the advantage of fast Li⁺ pseudocapacitive electrode material (T-Nb₂O₅). Cycling stability is another critical parameter of supercapacitor device. To demonstrate the long term stability of C-T-Nb₂O₅//AC hybrid supercapacitor device, we performed the cycling test using cyclic voltammetry at a scan rate of 20 mV s⁻¹. As shown in Fig. 4d, the specific capacitance could maintain 82.3% after 3000 cycles, indicated a good stability of this hybrid device. Meanwhile, the coulombic efficiency maintained 99% after a few hundred cycles, suggesting well balanced charge storage of cathode and anode reactions. Based on the previous discussion, the outstanding performance of hybrid supercapacitor can be attributed to the following reasons: 1) the high rate Li⁺ intercalation/deintercalation in orthorhombic phase; 2) the short Li⁺ diffusion length and facile electron transport brought about by ultrathin 1D nanowire structure; 3) stable electrochemical performance achieved by polydopamine derived carbon on T-Nb₂O₅ material.

Conclusion

In conclusion, this work provides an alternative method to fabricate Nb₂O₅ nanowire material using niobium oxalate coordination chemistry, which is highly adaptable to various substrates. T-Nb₂O₅ nanowires could be obtained through heat treatment. Especially for electrochemical energy storage application, the carbon coated T-Nb₂O₅ nanowire material exhibited high rate pseudocapacitive Li⁺ storage performance with high cycling stability. A prototype of 3 V hybrid supercapacitor using pseudocapacitive carbon coated T-Nb₂O₅//AC hybrid supercapacitor device was successfully fabricated with high energy density, power density as well as high stability. Future exploration of high performance pseudocapacitive Li⁺ ion storage electrode will be critical to develop next generation hybrid supercapacitors.

Acknowledgments

This work is conducted by NTU-HUJ-BGU Nanomaterials for Energy and Water Management Programme under the Campus for Research Excellence and Technological Enterprise (CREATE), that is supported by the National Research Foundation, Prime Minister's Office, Singapore.

Appendix A. Supporting information

Supplementary data associated with this article can be found in the online version at <http://dx.doi.org/10.1016/j.nanoen.2014.11.020>.

References

- [1] A. Burke, *Electrochim. Acta* 53 (2007) 1083-1091.
- [2] K. Naoi, S. Ishimoto, J.i. Miyamoto, W. Naoi, *Energ. Environ. Sci.* 5 (2012) 9363-9373.
- [3] Z. Chen, V. Augustyn, J. Wen, Y. Zhang, M. Shen, B. Dunn, Y. Lu, *Adv. Mater.* 23 (2011) 791-795.
- [4] J. Ni, L. Yang, H. Wang, L. Gao, *J. Solid State Electr.* 16 (2012) 2791-2796.
- [5] V. Aravindan, N. Shubha, W.C. Ling, S. Madhavi, *J. Mater. Chem. A* 1 (2013) 6145-6151.
- [6] V. Augustyn, J. Come, M.A. Lowe, J.W. Kim, P.L. Taberna, S. H. Tolbert, H.D. Abruña, P. Simon, B. Dunn, *Nat. Mater.* 12 (2013) 518-522.
- [7] J.W. Kim, V. Augustyn, B. Dunn, *Adv. Energ. Mater.* 2 (2012) 141-148.
- [8] X. Wang, G. Li, Z. Chen, V. Augustyn, X. Ma, G. Wang, B. Dunn, Y. Lu, *Adv. Energ. Mater.* 1 (2011) 1089-1093.
- [9] J. Yan, E. Khoo, A. Sumboja, P.S. Lee, *ACS Nano* 4 (2010) 4247-4255.
- [10] C.K. Chan, H. Peng, G. Liu, K. Mcllwraith, X.F. Zhang, R. A. Huggins, Y. Cui, *Nat. Nanotechnol.* 3 (2007) 31-35.
- [11] J.H. Kang, Y. Myung, J.W. Choi, D.M. Jang, C.W. Lee, J. Park, E.H. Cha, *J. Mater. Chem.* 22 (2012) 8413-8419.
- [12] B. Varghese, S.C. Haur, C.T. Lim, *J. Phys. Chem. C* 112 (2008) 10008-10012.
- [13] H. Wen, Z. Liu, J. Wang, Q. Yang, Y. Li, J. Yu, *Appl. Surf. Sci.* 257 (2011) 10084-10088.
- [14] A.L. Viet, M.V. Reddy, R. Jose, B.V.R. Chowdari, S. Ramakrishna, *J. Phys. Chem. C* 114 (2009) 664-671.
- [15] J.M. Jehng, I.E. Wachs, *J. Raman Spectrosc.* 22 (1991) 83-89.
- [16] Z.S. Wu, W. Ren, L. Wen, L. Gao, J. Zhao, Z. Chen, G. Zhou, F. Li, H.M. Cheng, *ACS Nano* 4 (2010) 3187-3194.
- [17] T. Ohzuku, K. Sawai, T. Hirai, *J. Power Sources* 19 (1987) 287-299.
- [18] K.T. Nam, D.W. Kim, P.J. Yoo, C.Y. Chiang, N. Meethong, P. T. Hammond, Y.M. Chiang, A.M. Belcher, *Science* 312 (2006) 885-888.
- [19] A. Le Viet, M.V. Reddy, R. Jose, B.V.R. Chowdari, S. Ramakrishna, *J. Phys. Chem. C* 114 (2010) 664-671.
- [20] X. Wang, W.S. Liu, X. Lu, P.S. Lee, *J. Mater. Chem.* 22 (2012) 23114-23119.
- [21] Z. Fan, J. Yan, T. Wei, L. Zhi, G. Ning, T. Li, F. Wei, *Adv. Funct. Mater.* 21 (2011) 2366-2375.
- [22] V. Khomenko, E. Raymundo-Pinero, F. Beguin, *J. Power Sources* 153 (2006) 183-190.